Nanofibers of solid-solution thorium(IV)-uranium(IV) oxides by electrospinning

Vojtech Kundrat, Vit Vykoukal, Zdenek Moravec, Jiri Pinkas*

Department of Chemistry, Faculty of Science, Masaryk University, Kotlarska 2, CZ-61137 Brno, Czech Republic

ABSTRACT

Thorium-uranium dioxide nanofibers were prepared in a three-step process. Green composite microfibers were electrospun from solutions composed of Th(IV) and U(VI) acetylacetonate complexes in different molar ratios, polyvinylpyrrolidone, and acetone/ethanol mixed solvents. The second step converted the green composite fibers by calcination in the air to mixed Th/U oxide fibers. In the final step, the heat treatment under forming gas provided the nanofibers with diameters of 28−46 nm composed of solid solutions $Th_xU_{1-x}O_2$ ($x = 1$, 0.75, 0.5, 0.25, 0). The XRD and STEM-EDS analyses of the prepared Th/U mixed oxide nanofibers attested to their atomic homogeneity.

© 2022 Elsevier B.V. All rights reserved.

1. Introduction

Nanoscopic actinide materials, mainly thorium and uranium oxides, attract attention due to their potential use as nanocrystalline material precursors for nuclear fuel in advanced heavy water reactors [1–3]. ThO_2 and UO_2 are isostructural, crystallize in fluorite lattice, and form solid solutions over the entire compositional range. Nanocrystalline thorium-uranium mixed oxides are interesting candidates for nuclear fuel usage with advantages over traditional fuel [4–6]. The main reasons for research efforts in this area are lowering the sintering temperature and enhancing material properties of the final sintered pellet, such as thermal conductivity, mechanical properties, plasticity, stress resistance, radiation damage resistance, and fission gas retention [7]. Most of these nanomaterials are desired in the form of nanoparticles because of their ideal spherical shape, which allows effective sintering [8]; however, the polycrystalline nanofibrous form could also be potentially valuable with its unique morphological properties [9].

Relatively high surface area and open fibrous structure predict usability for heterogeneous catalysis and sorption [10–12]. Nanofibers are also well-known for their utility in preparing composites [13]. Purely inorganic nanofibers, when carefully handled, should be safer than ultrafine particulate powders due to the flaky or bulky nature of nonwoven webs. Organic and inorganic nanofibers are nowadays industrially produced via needleless electrospinning providing high volumes of materials [14].

There are several reported preparation methods for nanoscopic mixed oxides of uranium and thorium. Hydrothermal and thermal decomposition of oxalates, prepared by coprecipitation of uranium(IV) and thorium(IV) solutions, was used in a sintering study and mechanical analysis of pellets produced by the spark plasma sintering technique [15]. In another study, mixed oxide nanocrystals were prepared by hot injection of thorium acetylacetonate and uranyl acetate solutions into hot benzyl ether. Various shapes and morphologies of nanocrystalline oxides were obtained [16]. Pure thorium and uranium dioxides and their solid solutions were prepared by the photochemical reaction of uranyl and thorium nitrates in an aqueous solution of ammonium formate. For the decomposition of mixed oxides, a mercury UV lamp was used [17].

Recently, we introduced the electrospinning route to nanofibrous uranium [18] and thorium [19] oxides. Others used the same method to prepare nanofibers containing uranium carbide [20]. Based on the experience with electrospinning processing of thoria and urania, we present here a facile preparation route to atomically mixed ThO_2/UO_2 oxides to enlarge the family of nanocrystalline nuclear materials.

---

* Corresponding author.
  E-mail address: jpinkas@chemi.muni.cz (J. Pinkas).

Table 1
Electrospinning solution compositions.

Solution parameter	A	B	C	D	E
Th/U ratio (molar)	1:0	3:1	1:1	1:3	0:1
Th(acac)$_4$ [g]	1.00	0.80	0.57	0.31	0
UO$_2$(acac)$_2$ [g]	0	0.20	0.43	0.69	1.00
PVP [g]			1.00		
EtOH [g]			18.0		
Acetone [g]			10.0		

2. Experimental procedures

2.1. General

Polyvinylpyrrolidone (PVP, $M_w = 360$ kDa) was purchased from Sigma Aldrich and used as received. Uranyl acetylacetonate was synthesized according to the literature [21], and the typical procedure was already described in the previous study [18]. Thorium acetylacetonate was synthesized according to the literature [22] from thorium nitrate tetrahydrate (98%, Lachema, CZ). Acetone and ethanol (absolute) were purchased from Penta Chemicals (CZ) in a p.a. quality and used without further workup. Forming gas with a composition of 5% of H$_2$ in N$_2$ was used for reductions.

2.2. Preparation of electrospinning solutions and electrospinning

Thorium acetylacetonate, uranyl acetylacetonate hydrate, and PVP were dissolved in a mixture of acetone and ethanol in various mass ratios (solutions A − E, Table 1). The solutions were stirred for 2 h, characterized, transferred to a syringe pump, and electrospun. The solutions were prepared based on different ratios of the thorium/uranium content. The actual compositions and corresponding chemical and physical characteristics of the electrospinning solutions are shown in Table 1.

The process was conducted on a custom-designed set-up [18] based on two high-voltage power sources capable of an output of 0 to +25 kV and 0 to −15 kV and on a New Era Scientific syringe pump. The syringe with a blunt-tip needle of 1 mm diameter was used as a carrier of the spinning solution. A negative-charge source was connected to the collector electrode, a circular metal plate with a diameter of 200 mm. Fibers were collected on the collector covered by aluminum foil which helped the manipulation of the samples. Experiments were performed in a fume hood in an air-conditioned laboratory with a fixed temperature of 296 ± 2 K and relative humidity of $40 \pm 10\%$. Electrospinning parameters are presented in Table 2.

2.3. Calcination and reduction treatment

After the electrospinning process, in which green composites of thorium and uranyl acetylacetonates and PVP polymer were formed, the calcination step was performed to obtain purely inorganic fibers. A muffle furnace set to 773 K with an ambient air atmosphere was used for oxidative treatment. In all cases, the heating rate was set to achieve the maximum calcination temperature in 4 h, followed by another 4 h dwell time, and finished by spontaneous cooling down to an ambient temperature. After the heat

Table 2
Electrospinning parameters.

High voltage (+) [kV]	High voltage (−) [kV]	Flow rate [μl min^{-1}]	Electrode distance [mm]
15.0 ± 0.1	-10 ± 0.1	50	150

treatment, calcined materials were collected and analyzed. A horizontal tube furnace equipped with a quartz tube was used for a reduction treatment. The same maximum temperatures and heating program were used as in the case of calcination in air. The reduction was performed on materials peeled off from the aluminum foil support. A continuous H$_2$/N$_2$ gas flow was delivered from a gas cylinder and controlled by a silicon oil bubbler attached to the quartz tube at the outlet. Two different maximum temperatures were selected (873 and 1073 K). The heating ramp of 4 h with another 4 h dwell time was used, and the process was completed by cooling down to ambient temperature.

2.4. Characterization

The prepared nanofibrous materials were characterized by scanning electron microscopy (SEM) and transmission electron microscopy (TEM). The samples for the TEM measurements were dispersed in methanol, and 4 μl of the suspension was placed on a Quantifoil copper grid and allowed to dry by evaporation at ambient temperature. TEM characterizations were performed on an FEI Tecnai G2 microscope at 200 kV equipped with a 4k CCD camera FEI Eagle. Micrographs were analyzed by the ImageJ software for the fiber diameter and size distribution.

The STEM-EDS measurements were performed on an FEI Titan Themis instrument with a combination of a spherical aberration image (Cs) corrector, a monochromator system, sensitive ChemiSTEM technology, and a high-end GATAN GIF Quantum energy filter for EELS and EFTEM with a new enhanced piezo stage, FEI and GATAN software, and an FEI Ceta 16-megapixel CMOS camera. STEM-EDS figures were processed by the Velox software. The distribution of elements is illustrated based on the signal intensity.

Thermogravimetric, differential scanning calorimetry (TG/DSC), and differential thermal analysis in reducing atmosphere of forming gas (TG/DTA) were performed on a Netzsch Jupiter STA 449 instrument with a heating rate of 10 K min^{-1} and a maximum temperature of 1273 K. The measurements in air were performed using a DSC holder with a Pt/Rh sensor while the measurements in the atmosphere of forming gas were done with a DTA holder with a W/*Re* sensor. Reducing atmosphere was purified by passing through a deoxygenation cartridge and by a Zr getter.

X-ray powder diffraction (XRD) measurements were performed on an Empyrean diffractometer (PanAnalytical) with a Co ($\lambda_{K\alpha} = 1.79030$ Å) X-ray lamp at room temperature. The phase composition was determined by the Rietveld computation with the evaluation of crystalline size by the Scherrer equation with HighScorePlus 4.0 (PanAnalytical) equipped by a model from the ICSD database.

3. Results and discussion

For the synthesis, acetylacetonate complexes of Th(IV) and U(VI) were selected due to their excellent solubility in organic solvents and good compatibility with polyvinylpyrrolidone (PVP). The mixture of acetone and ethanol was used as a solvent. Five electrospinning solutions were prepared with different thorium/uranium ratios. The solutions A and E represent precursors for pure thoria ThO$_2$ and urania UO$_2$, respectively, and the solutions B, C, and D have the Th/U ratios of 3:1, 1:1, 1:3, respectively. After the dissolution of both PVP polymer and inorganic precursors, slightly viscous solutions with a range of colors from off-white (solution A) to bright orange (solution E) with different shades of yellow in between (solutions B, C, and D) corresponding with uranium content were obtained.

The electrospinning of the precursor solutions delivered white (solution A) and yellowish (solutions B-E) paper-like materials, which were collected on aluminum foil and analyzed by SEM (Fig.
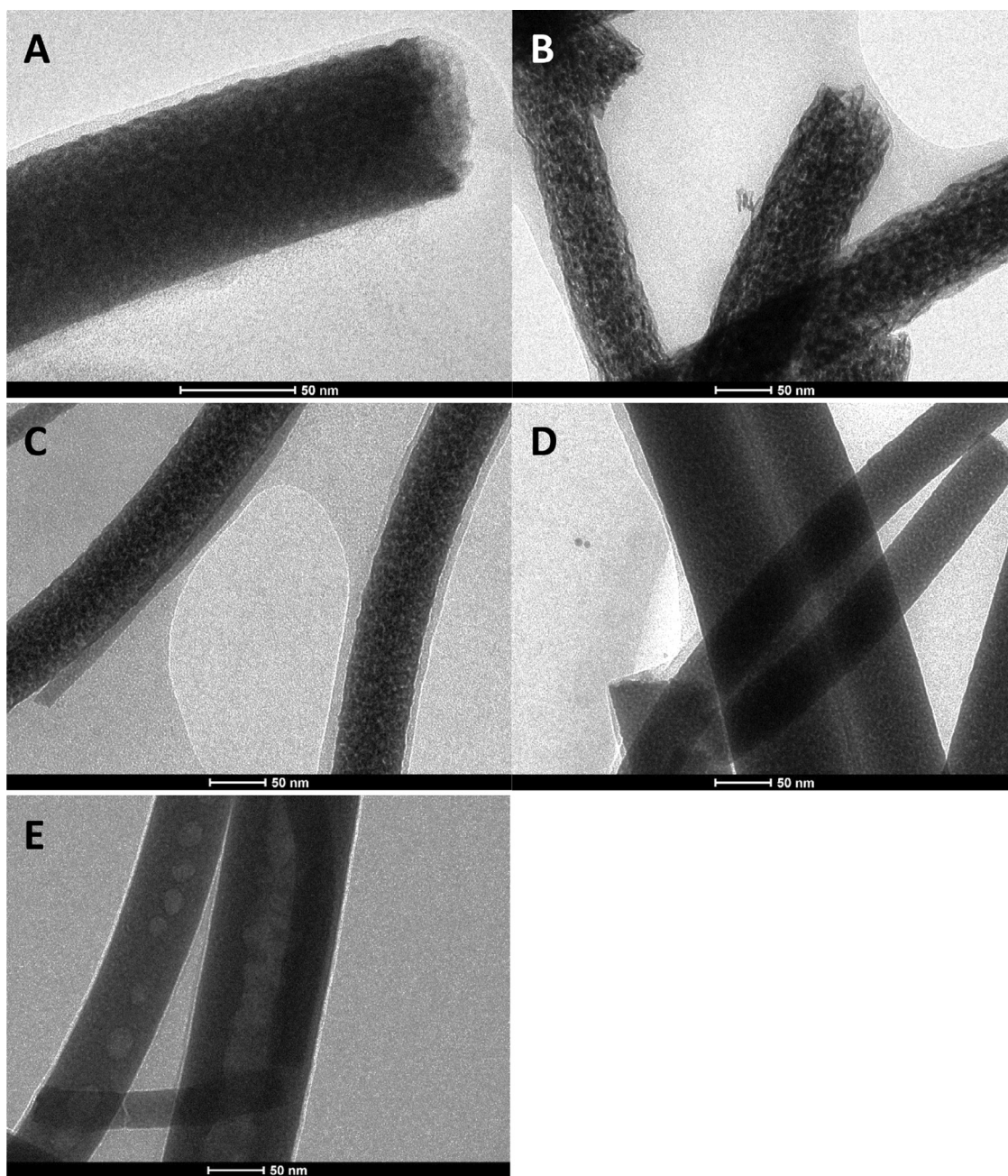
Fig. 1. TEM images of calcined fibers at 773 K with various molar ratios of Th and U: A (1:0), B (3:1), C (1:1), D (1:3), E (0:1).

Table 3
The average diameter [nm] of prepared Th/U oxide fibers.

Sample	A	B	C	D	E
Nominal composition	ThO_2	$Th_{0.75}U_{0.25}O_2$	$Th_{0.50}U_{0.50}O_2$	$Th_{0.25}U_{0.75}O_2$	UO_2
Green fibers	184 ± 95	181 ± 87	190 ± 61	203 ± 68	225 ± 100
Oxidized at 773 K	36 ± 13	47 ± 17	56 ± 18	67 ± 22	99 ± 36
Reduced at 873 K	–	46 ± 19	28 ± 18	45 ± 25	46 ± 24
Reduced at 1073 K	–	29 ± 12	30 ± 18	48 ± 19	45 ± 18

1S, 2S in the Supplementary materials) and TG-DSC analysis (Fig. 3S). The analysis of obtained micrographs provided average diameters of green fibers, which are shown in Table 3.

In all cases, the electrospinning provided smooth organic-based submicron fibers with a relatively broad distribution of diameters; however, the moderate trend of the increase of the mean diameter with the addition of uranyl acetylacetonate could be observed.

Histograms of fiber diameters are presented in the Supplementary materials (Fig. 2S).

The TG-DSC analysis in the air provided insight into the calcination process and established a proper temperature to remove organic polymer completely and leave purely inorganic oxidized fibers. In all samples, mass loss occurs at temperatures between 550 and 800 K (Fig. 3S). In some cases (samples C, D, and E),
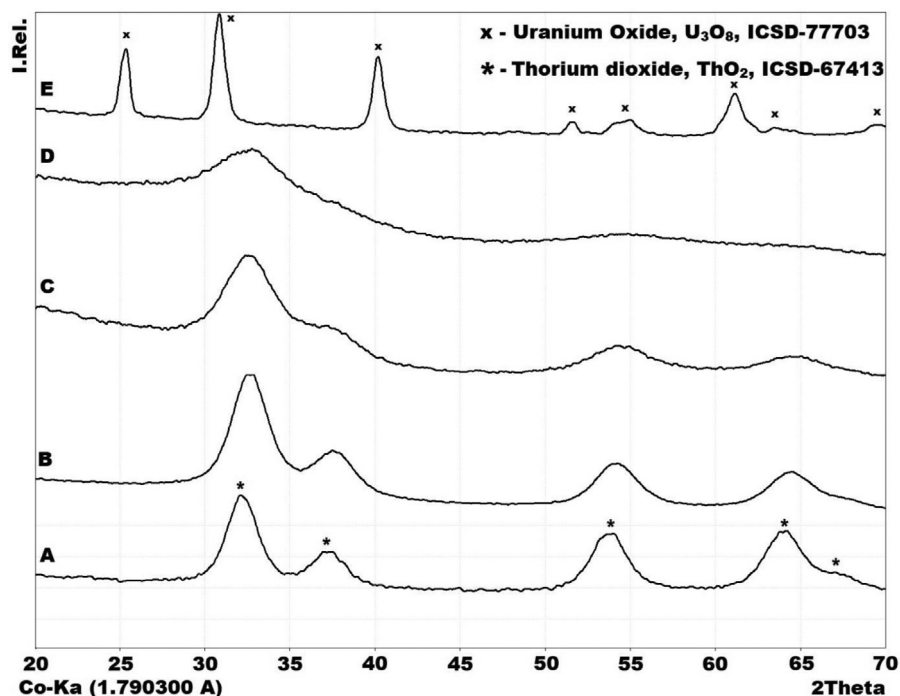
Fig. 2. XRD analysis of calcined fibers with various molar ratios of Th and U: A (1:0), B (3:1), C (1:1), D (1:3), E (0:1).
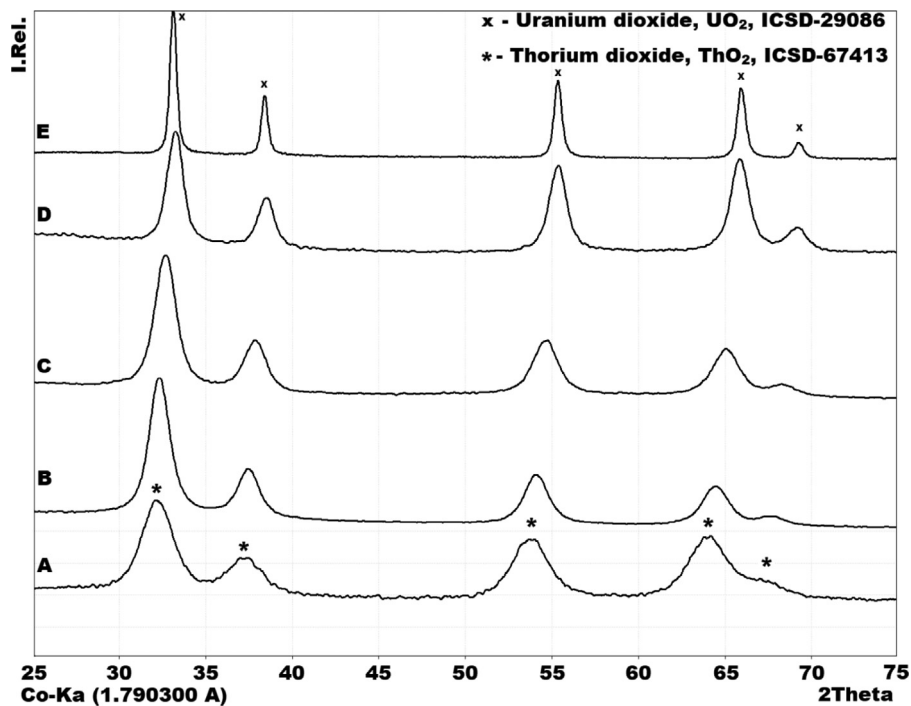

Fig. 3. XRD analysis of reduced fibers at 873 K in forming gas atmosphere with various molar ratios of Th and U: A (1:0), B (3:1), C (1:1), D (1:3), E (0:1).

the calcination process showed two conspicuous exothermic mass losses, while the rest of the samples (A, B) displayed only one. In the case of sample D, exothermic mass loss occurs at 573 K, followed by a slight mass loss at approximately 700 K after which it reaches a constant mass. For sample E, the final constant mass was achieved above 773 K, which was the highest value, and thus it was selected as the calcination temperature for the subsequent calcination treatment.

The calcination treatment of bulk green fibers was performed in a muffle furnace under air at 773 K in alumina crucibles, where

fibers on the aluminum foil were placed. After burnout, the samples were collected as white (sample A), yellowish (samples $B - D$), and greenish (sample E) brittle layers deposited on aluminum sheets. The samples were analyzed by the SEM (Fig. 4S), TEM (Fig. 1), and XRD (Fig. 2) methods. Average diameters of calcined fibers are presented in Table 3, and corresponding histograms are shown in the Supplementary materials (Fig. 5S).

The SEM analysis (Fig. 4S) provided the average diameters of fibers. There is a considerable decrease in fiber width after calcination, the most profound for ThO_2. The fiber diameter increases
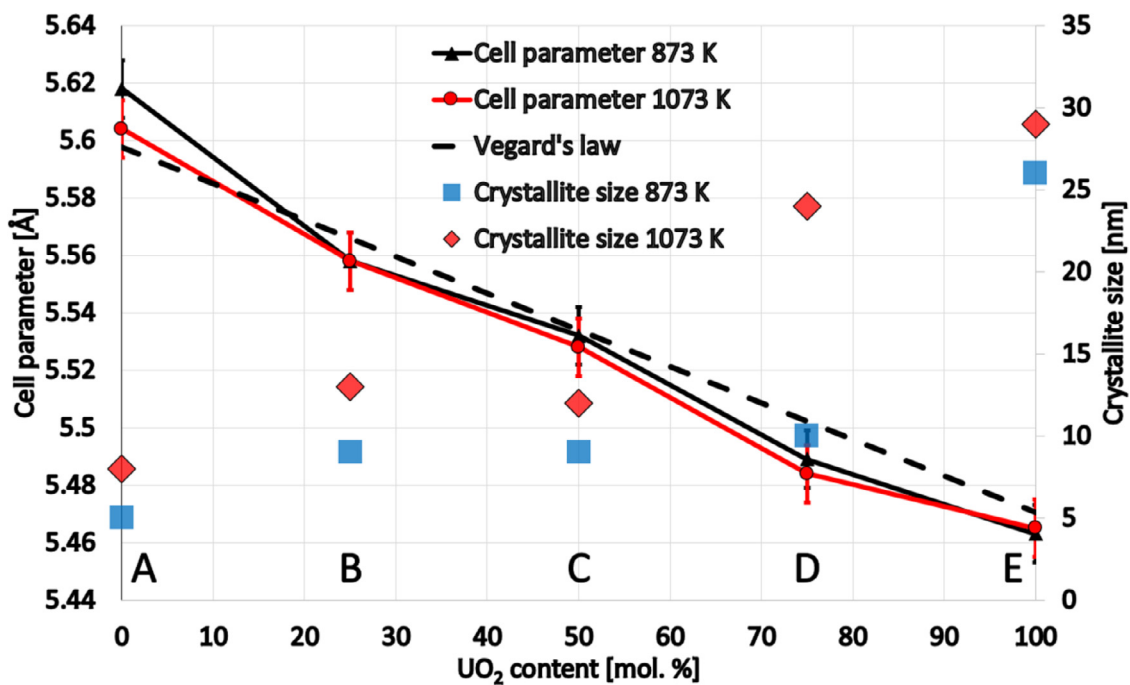
Fig. 4. Dependence of the cell parameter on uranium dioxide content in mixed ThO_2/UO_2 nanofibers and their crystallite size. Samples reduced at 873 K (■) and 1073 K (♦). Molar ratios of Th and U: A (1:0), B (3:1), C (1:1), D (1:3), E (0:1).
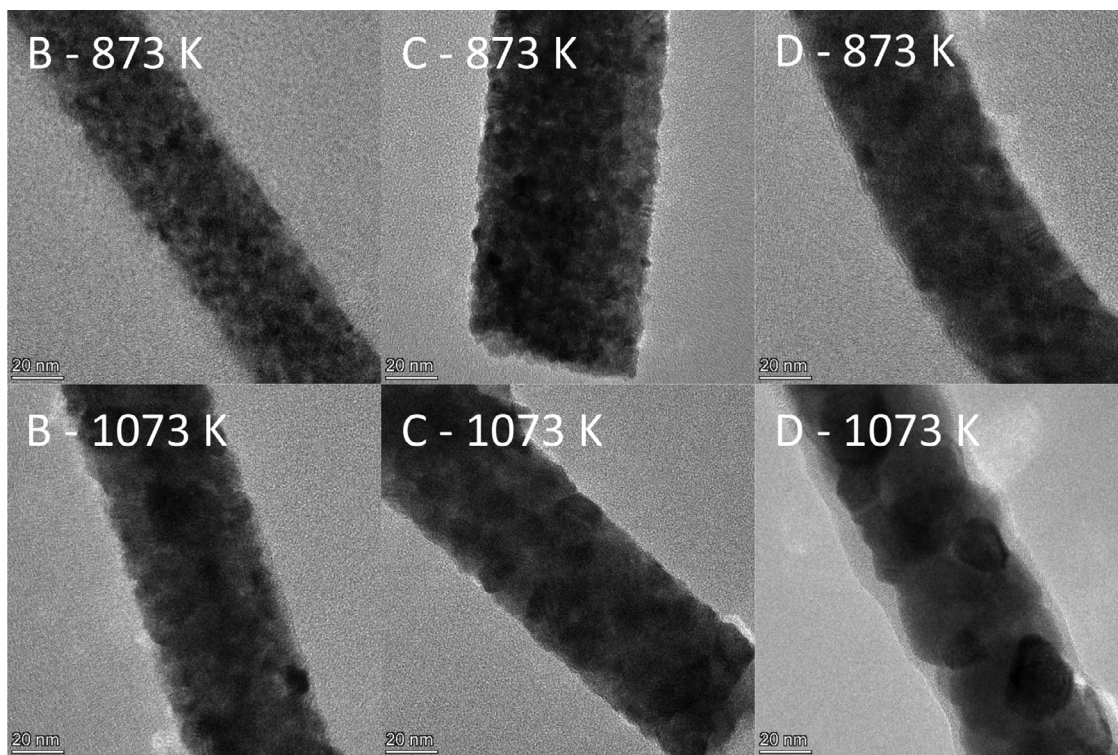

Fig. 5. TEM analysis of reduced $Th_xU_{1-x}O_2$ nanofibers. Samples reduced at 873 K (B − D 873 K) and 1073 K (B − D 1073 K).

with increasing uranium content. While pure ThO_2 (sample A, Fig. 4SA) resulting from oxidation of the green composite has a diameter in the nanoscopic range (36 nm), its counterpart consisting of pure uranium oxide (sample E, Fig. 4SE) provides substantially thicker fibers of 99 nm; however, their thickness is still mostly under 100 nm. In mixed Th/U oxide fibers, we observed a steady increase in fiber diameter corresponding with increasing uranium proportion. While the morphology of the fibers inspected by SEM seems in all cases similar, the TEM analysis (Fig. 1) provided insight into the inner morphology, which differs fundamentally for different compositions. Pure ThO_2 (sample A, Fig. 1A) and uranium oxide (sample E, Fig. 1E), as already described in our previous studies [18,19], show internal porosity. Thoria consists of homogeneously porous matter, while uranium oxide shows a partially hollow character of the fibers. With the addition of uranium (sample B, Fig. 1B), the character of observable porosity changed into
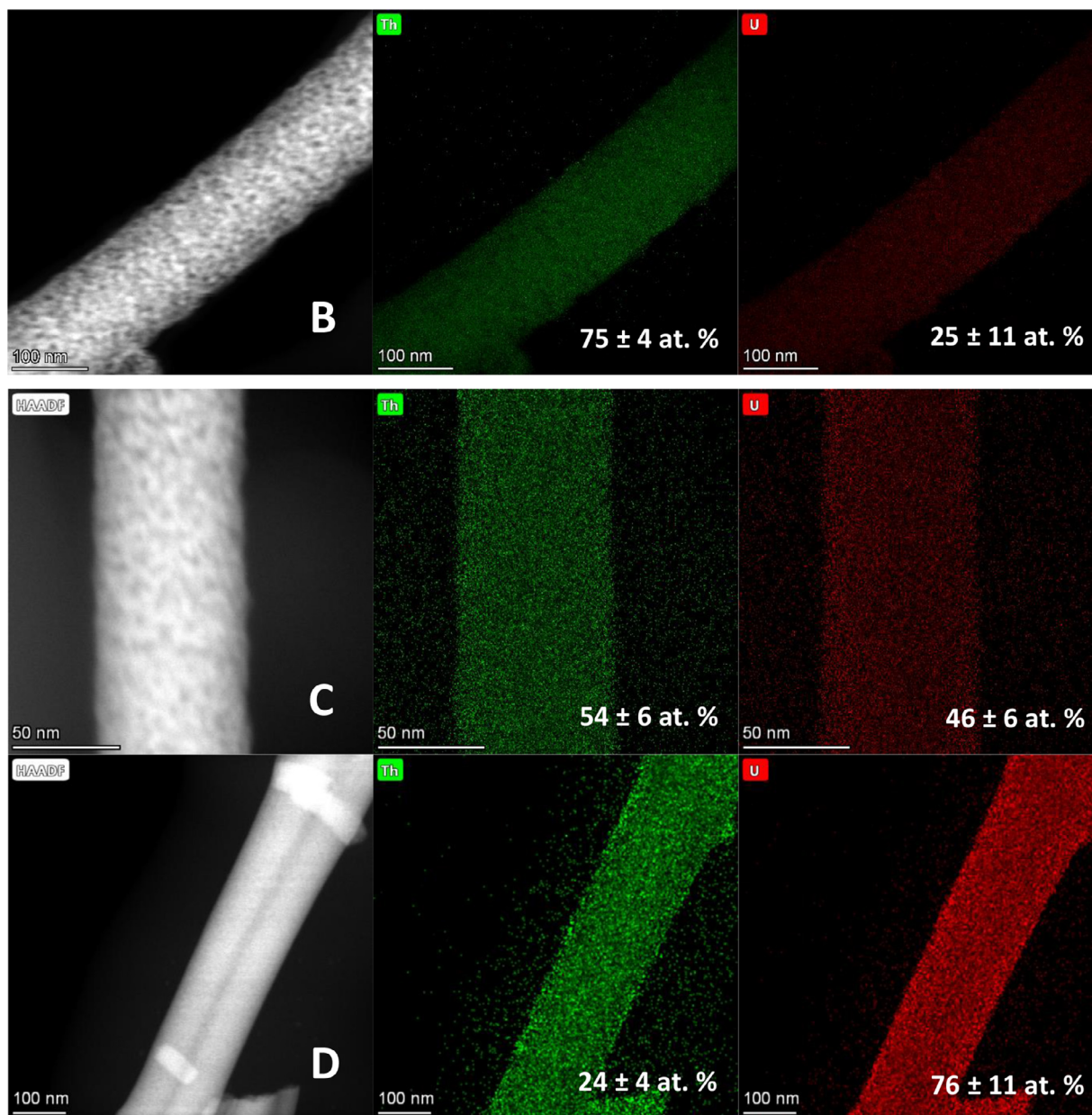
Fig. 6. STEM-EDS analysis of mixed oxide ThO_2/UO_2 nanofibers, HAADF mode, and chemical mapping mode (Th – green; U – red), the atomic percentage in the form of Th/U ratio. Molar ratios of Th and U: B (3:1) top, C (1:1) middle, D (1:3) bottom.

flake-like grains. The sample consisting of thorium and uranium in 1:1 and 1:3 ratios (sample C, D, Fig. 1C, D, respectively) lost the character of the previous sample, and the fibers consisted of ultra-fine grains.

The XRD analysis (Fig. 2) of samples A and E provided diffractograms of pure cubic thoria and uranium oxide U_3O_8, respectively. Thoria adopts a CaF_2-type structure, while uranium oxide is in the form of U_3O_8 as the stable oxidation state. The samples B, C, and D adopt the CaF_2 structure, which indicates solubility of uranium in the fluorite lattice of ThO_2 and a transition to the amorphous character of Th/U oxides in the samples. With the increased uranium content in the samples, individual diffractions are broader and less intense. This tendency culminates in the diffractogram of sample D (Fig. 2D).

The transformation of the calcined fibers to the final state of $Th_xU_{1-x}O_2$ solid solution was accomplished by a reduction treatment. To establish a proper reduction temperature, we analyzed the samples by the TG-DTA method in forming gas (Fig. 6S). All samples were treated at a steadily increasing temperature of 10 K min^{-1} up to 1273 K. In all cases, except the sample A of pure thoria, the mass decrease was observed below 1000 K. In the cases of pure uranium oxide and the sample D with a 1:3 ratio of Th/U (Fig. 6SE and D, respectively), the final mass was reached at approximately 900 K. In the samples with a lower uranium content (Fig. 6SB, C), the mass decrease was completed at even lower temperature of 800 K. Based on these observations, two reduction temperatures were selected at 873 K and 1073 K to compare their potential influence on the fiber diameter and morphology. The reduction treatments were performed in a tube furnace under the continuous forming gas flow. After reduction, gray powdery materials were collected and analyzed by the SEM (Fig. 7S, 8S), XRD (Fig. 3, 873 K, and Fig. 9S, 1073 K), TEM (Fig. 5), and STEM-EDS (Fig. 6) methods. Obtained micrographs (Fig. 7S) were compared to the effects of different reduction temperatures and various Th/U ele-

mental ratios. Average diameters of the fibers were measured, and corresponding histograms are shown in Fig. 8S.

All prepared materials appear similar except for pure UO_2 samples (Fig. 7SG, H), where the crystalline character of fibers is more pronounced than in other cases, which have relatively smooth surfaces. All fibrous samples are comparable in their average diameter (Table 3) and size distributions (Fig. 8S), where most of the fibers have a diameter lower than 50 nm.

The XRD analysis provided diffractograms of prepared materials where the trend in the Th/U atomic ratio is observable on individual diffractions shifts from pure thoria to pure urania. The sample A reduced at 873 K (Fig. 3A) consisting of pure thoria (ICSD-67413) was not treated in forming gas due to its final oxidation state and is presented for comparison. In mixed samples of urania and thoria (Fig. 3B−D), broad diffractions of the fluorite structural type are present. Compared with calcined samples (Fig. 2), it is possible to see more intense signals due to the higher crystallinity of the prepared solid solutions. The pure urania (ICSD-29086) sample (Fig. 3E) features narrower signals than other samples from the series.

Similarly, analysis of the $Th_xU_{1-x}O_2$ nanofibers at 1073 K (Fig. 9S) provided identical diffractions patterns with the main difference of narrower signals due to the higher treatment temperature that resulted in the growth of crystallites.

The analysis of XRD patterns provided the lattice constants and particle sizes displayed in Fig. 4 and tabulated in the Supplementary materials (Table 1S). The lattice parameters reveal dependence on the Th/U content, and the obtained data approximately follow Vegard's law [23,24,25], except for higher uranium-containing sample D with a smaller cell parameter which correspond with the study on micro-and nanoparticles of the same material [15]. The deviation from the law is explained by partial oxidation of the samples in the air. Additional possible reasons could be partial phase separation of UO_2 from the $Th_xU_{1-x}O_2$ solid solution, defect formation, and deviation from an ideal oxygen stoichiometry. At the other end of the series, pure thoria (Fig. 4, point A) also differs from the reported values ($a = 5.5975$ Å). The possible explanation could be the impurities remaining in the structure after the oxidation process of PVP.

The size of crystallites brought significant insight into the process. The smallest crystallites could be found in the pure thoria sample (Fig. 4, point A) after the reduction treatment at both 873 and 1073 K with a slight increase at higher of these two temperatures. Crystallites of mixed-oxide samples B, C, and D, are similar and nearly twice as big as in pure thoria samples. Pure uranium dioxide (Fig. 4, point E) has a much larger crystallite size due to the absence of size stabilizing effect of thoria lattice as in other samples. The comparison of the crystallite sizes (Fig. 4) shows the difference of the reduction processes at 873 and 1073 K for sample D. While the samples B and C with relatively high thorium content remain similar in crystallite size at both temperatures, the sizes of products differ substantially in sample D. The sample D processed at 873 and 1073 K has crystallite sizes 10 and 24 nm, respectively. Thoria lattice acts as a stabilizing structure during the reduction process, while in the case of low thoria content, the stabilizing effect is weaker at higher temperatures, and crystallites are enlarged. The sample E consisting of pure urania shows even larger but similar sizes at both reduction temperatures.

The approximate estimation of crystallite size from the Scherrer equation based on the XRD measurement was compared with the TEM analysis (Fig. 5). In all cases, polycrystalline structures were observed with ultrafine nanofiber-forming particles. Samples prepared at 873 K have a similar crystallite size smaller than 10 nm in diameter (Fig. 5B−D 873 K). By reduction at 1073 K, the crystallite size is slightly enlarged in the case of samples B and C (Fig. 5B, C 1073 K). The case of sample D (Fig. 5D 1073 K) reduced at 1073 K corresponds closely to the Scherrer equation result (Fig. 4D 1073 K)

where substantially enlarged crystallites were detected. The observed particles are much more distinct than in the case of the sample reduced at 873 K.

We performed the STEM-EDS analysis to prove the homogeneity of element distribution and inner structure of the prepared mixed oxide $Th_xU_{1-x}O_2$ nanofibers (Fig. 6). Thorium/uranium ratios calculated from atomic fractions from the EDS analysis are presented in Fig. 6 in corresponding elemental mappings. Visualization of the analysis of samples B, C, and D is divided into three sections, i.e., HAADF, thorium, and uranium chemical mapping visualized in green and red color, respectively. All samples display a homogenous character of the fibers; however, with different inner morphology, corresponding with the previous inner structure of unreduced precursors. Sample B has apparent inner porosity, which is diminished in sample C and completely disappears in sample D. In the same cases, hollow fibers are observable (Fig. 6D, HAADF). The elemental ratios of thorium and uranium calculated from the EDS analysis correspond with the nominal compositions of the electrospinning solutions.

4. Conclusion

For the first time, nanofibers of solid-solution thorium-uranium dioxide were prepared by the electrospinning method. The preparation relies on a three-step process where electrospinning of polymer solutions containing a mixture of precursors of thoria and urania was followed by oxidative calcination of green fibers and their further reduction treatment at elevated temperatures to monophasic $Th_xU_{1-x}O_2$ ($x = 1, 0.75, 0.5, 0.25, 0$). Trends in the fiber diameter during the preparation were observed. The electrospinning process provided relatively thick fibers that were converted by oxidative treatment to fibers in the nanoscopic range. A further reduction provided even thinner fibers of mixed $Th_xU_{1-x}O_2$ oxides with a mean diameter less than 50 nm for all examined Th/U ratios. The XRD and STEM-EDS analysis proved chemical and phase composition, which allowed constructing a diagram with Vegard's law dependence of the lattice parameter on the Th/U content. The prepared materials enlarge the family of nanoscopic nuclear materials, which could find usability in the nuclear industry, heterogeneous catalysis, or as a matrix for the sorption of highly active materials.

Declaration of Competing Interest

The authors declare that they have no known competing financial interests or personal relationships that could have appeared to influence the work reported in this paper.

Supplementary materials

Supplementary material associated with this article can be found, in the online version, at doi:10.1016/j.jnucmat.2022.153731.

References

[1] T.M. Nenoff, B.W. Jacobs, D.B. Robinson, P.P. Provencio, J. Huang, S. Ferreira, D.J. Hanson, Synthesis and Low Temperature In Situ Sintering of Uranium Oxide Nanoparticles, Chem. Mater. 23 (2011) 5185–5190, doi:10.1021/cm2020669.

[2] V. Tyrpekl, M. Cologna, D. Robba, J. Somers, Sintering behaviour of nanocrystalline ThO_2 powder using spark plasma sintering, J. Eur. Ceram. Soc. 36 (2016) 767–772, doi:10.1016/j.jeurceramsoc.2015.11.006.

[3] V. Tyrpekl, M. Cologna, J.-.F. Vigier, A. Cambriani, W. De Weerd, J. Somers, Preparation of bulk-nanostructured UO_2 pellets using high-pressure spark plasma sintering for LWR fuel safety assessment, J. Am. Ceram. Soc. 100 (2017) 1269–1274, doi:10.1111/jace.14647.

[4] J.S. Herring, P.E. MacDonald, K.D. Weaver, C. Kullberg, Low cost, proliferation resistant, uranium–thorium dioxide fuels for light water reactors, Nucl. Eng. Des. 203 (2001) 65–85, doi:10.1016/S0029-5493(00)00297-1.

[5] M. Saoudi, D. Staicu, J. Mouris, A. Bergeron, H. Hamilton, M. Naji, D. Freis, M. Cologna, Thermal diffusivity and conductivity of thorium-uranium mixed oxides, J. Nucl. Mater. 500 (2018) 381–388, doi:10.1016/j.jnucmat.2018.01.014.

[6] N. Hingant, N. Clavier, N. Dacheux, N. Barre, S. Hubert, S. Obbade, F. Taborda, F. Abraham, Preparation, sintering and leaching of optimized uranium thorium dioxides, J. Nucl. Mater. 385 (2009) 400–406, doi:10.1016/j.jnucmat.2008.12.011.

[7] J. Spino, H. Santa Cruz, R. Jovani-Abril, R. Birtcher, C. Ferrero, Bulk-nanocrystalline oxide nuclear fuels – An innovative material option for increasing fission gas retention, plasticity and radiation-tolerance, J. Nucl. Mater. 422 (2012) 27–44, doi:10.1016/j.jnucmat.2011.11.056.

[8] R. Chaim, G. Chevallier, A. Weibel, C. Estournès, Grain growth during spark plasma and flash sintering of ceramic nanoparticles: a review, J. Mater. Sci. 53 (2018) 3087–3105, doi:10.1007/s10853-017-1761-7.

[9] H. Esfahani, R. Jose, S. Ramakrishna, Electrospun Ceramic Nanofiber Mats Today: synthesis, Properties, and Applications, Materials (Basel) 10 (2017) 1238, doi:10.3390/ma10111238.

[10] Y. Dai, W. Liu, E. Formo, Y. Sun, Y. Xia, Ceramic nanofibers fabricated by electrospinning and their applications in catalysis, environmental science, and energy technology, Polym. Adv. Technol. 22 (2011) 326–338, doi:10.1002/pat.1839.

[11] S. Sundarrajan, A.R. Chandrasekaran, S. Ramakrishna, An Update on Nanomaterials-Based Textiles for Protection and Decontamination: an Update on Nanomaterials-Based Textiles, J. Am. Ceram. Soc. 93 (2010) 3955–3975, doi:10.1111/j.1551-2916.2010.04117.x.

[12] V. Thavasi, G. Singh, S. Ramakrishna, Electrospun nanofibers in energy and environmental applications, Energy Environ. Sci. 1 (2008) 205–221, doi:10.1039/b809074m.

[13] Z.-.M. Huang, Y.-.Z. Zhang, M. Kotaki, S. Ramakrishna, A review on polymer nanofibers by electrospinning and their applications in nanocomposites, Compos. Sci. Technol. 63 (2003) 2223–2253, doi:10.1016/S0266-3538(03)00178-7.

[14] L. Persano, A. Camposeo, C. Tekmen, D. Pisignano, Industrial Upscaling of Electrospinning and Applications of Polymer Nanofibers: a Review, Macromol. Mater. Eng. 298 (2013) 504–520, doi:10.1002/mame.201200290.

[15] L. Balice, D. Bouëxière, M. Cologna, A. Cambriani, J.-.F. Vigier, E. De Bona, G.D. Sorarù, C. Kübel, O. Walter, K. Popa, Nano and micro $U_{1-x}Th_xO_2$ solid solutions: from powders to pellets, J. Nucl. Mater. 498 (2018) 307–313, doi:10.1016/j.jnucmat.2017.10.042.

[16] D. Hudry, J.-.C. Griveau, C. Apostolidis, O. Walter, E. Colineau, G. Rasmussen, D. Wang, V.S.K. Chakravadhaluna, E. Courtois, C. Kübel, D. Meyer, Thorium/uranium mixed oxide nanocrystals: synthesis, structural characterization and magnetic properties, Nano Res 7 (2014) 119–131, doi:10.1007/s12274-013-0379-6.

[17] T. Pavelková, V. Čuba, F. Šebesta, Photo-induced low temperature synthesis of nanocrystalline UO_2, ThO_2 and mixed UO_2–ThO_2 oxides, J. Nucl. Mater. 442 (2013) 29–32, doi:10.1016/j.jnucmat.2013.08.016.

[18] V. Kundrat, A. Patak, J. Pinkas, Preparation of ultrafine fibrous uranium dioxide by electrospinning, J. Nucl. Mater. 528 (2020) 151877, doi:10.1016/j.jnucmat.2019.151877.

[19] V. Kundrat, Z. Moravec, J. Pinkas, Preparation of thorium dioxide nanofibers by electrospinning, J. Nucl. Mater. 534 (2020) 152153, doi:10.1016/j.jnucmat.2020.152153.

[20] S. Chowdhury, L. Maria, A. Cruz, D. Manara, O. Dieste-Blanco, T. Stora, A. Gonçalves, Uranium Carbide Fibers with Nano-Grains as Starting Materials for ISOL Targets, Nanomaterials 10 (2020) 2458, doi:10.3390/nano10122458.

[21] A.E. Comyns, B.M. Gatehouse, E. Wait, The chemistry of uranyl acetylacetone complex, J. Chem. Soc. (Resumed) (1958) 4655–4665, doi:10.1039/jr9580004655.

[22] R.C. Young, J. Kovitz, L.E. Marchi, Thorium Acetylacetonate (Tetrakis(2,4-Pentanediono)Thorium), in: W.C. Fernelius (Ed.), Inorganic Syntheses, John Wiley & Sons, Inc., Hoboken, NJ, USA, 2007: pp. 123–125. doi:10.1002/9780470132333.ch36.

[23] S. Hubert, J. Purans, G. Heisbourg, P. Moisy, N. Dacheux, Local Structure of Actinide Dioxide Solid Solutions $Th_{1-x}U_xO_2$ and $Th_{1-x}Pu_xO_2$, Inorg. Chem. 45 (2006) 3887–3894, doi:10.1021/ic050888y.

[24] G.W.C. Silva, J.D. Hunn, C. Yeamans, G.S. Cerefice, K.R. Czerwinski, Fluoride-Conversion Synthesis of Homogeneous Actinide Oxide Solid Solutions, Inorg. Chem. 50 (2011) 11004–11010, doi:10.1021/ic201552g.

[25] S. Anthonysamy, G. Panneerselvam, S. Bera, S.V. Narasimhan, P.R.V. Rao, Studies on thermal expansion and XPS of urania-thoria solid solutions, J. Nucl. Mater. 281 (2000) 15–21, doi:10.1016/S0022-3115(00)00185-9.